SUPPLEMENT TO THE *WELDING JOURNAL*, FEBRUARY 2011
**Sponsored by the American Welding Society and the Welding Research Council**

# Stray Grain Formation and Solidification Cracking Susceptibility of Single Crystal Ni-Based Superalloy CMSX-4

*Stray grain area fraction and cracking susceptibility were correlated to welding process and parameters*

**BY T. D. ANDERSON AND J. N. DUPONT**

**ABSTRACT**

The stray grain formation behavior and susceptibility to solidification cracking in autogenous welds on single crystal alloy CMSX-4 have been investigated. Welds were prepared using the electron beam (EB) and gas tungsten arc welding (GTAW) processes. The stray grain area fraction and cracking susceptibility were determined and correlated to the processing parameters and process type. The stray grain content initially increased and then decreased with increasing travel speed. This effect is attributed to the complex effect of travel speed on the temperature gradient and growth rate and resulting amount of constitutional supercooling in the weld. The stray grain content decreased with decreasing weld power. In general, the amount of stray grains and resultant cracking susceptibility were observed to decrease by the use of low heat inputs. The stray grain content and cracking susceptibility of welds prepared with the GTA process was always higher than welds made with the EB process. This difference is attributed to differences in power density and temperature gradient, where the EB process produced a higher temperature gradient that reduced the amount of stray grains and resultant susceptibility to cracking. For the conditions evaluated in this work, EB welds produced at heat inputs below ~ 13 J/mm produced welds that were crack-free with stray grain contents < 5 %.

## Introduction

Nickel-based single crystal superalloys are used for turbine blades for their excellent creep resistance. These materials are very expensive as a result of the complex fabrication conditions required to maintain the single crystal structure during casting. Some blades must be scrapped after casting because the formation of defective "stray" grains (SG), while other blades may need to be replaced after finite service exposures due to damage associated with wear, fatigue, or creep. Thus, there is a need to develop reliable welding techniques in order to rejuvenate damaged blades or repair blades with casting defects. This involves the establishment of welding parameters that will avoid the formation of SG in the weld. The SG formation tendency is a strong function of the local solidification conditions, which are controlled by the welding parameters. Another type of welding defect that is commonly observed in this class of alloys is solidification cracks. Solidification cracks are commonly associated with SG formation, but the particular range of welding parameters over which cracking can occur is not typically well established. The complex relations between welding parameters, solidification parameters, resultant SG formation, and solidification cracking susceptibility make the development of reliable weld repair strategies difficult.

*T. D. ANDERSON is a research engineer, ExxonMobil Upstream Research Co., Houston, Tex. J. N. DUPONT (*jnd1@lehigh.edu*), R. D. Stout Distinguished Professor, is with Lehigh University, Bethlehem, Pa.*

**KEYWORDS**

EB Process
GTAW Process
Cracking
Single Crystal
Stray Grains
Superalloy

### Stray Grain Development

Stray grain formation is known to be a result of constitutional supercooling (CS), which is controlled by temperature gradient (G) in the liquid directly ahead of the solid/liquid interface and the growth rate (V). Research has shown that a low G/V ratio will promote the nucleation of SG by introducing excessive liquid undercooling ahead of the solidifying columnar dendrite front (Ref. 1). There exists a wide range of G and V across the solidification interface of a weld pool. In a polycrystalline material, dendrite growth will generally be opposite to the direction of heat flow, so G and V are considered normal to the solid/liquid interface. For the case of a single crystal (SX) material, the growth directions are limited to one of the six crystallographic <100> easy growth vectors. The relevant G and V for SX solidification are those parallel to the local dendrite growth directions, $G_{hkl}$ and $V_{hkl}$. These can be calculated using a geometric model (Refs. 2–4) if the weld pool shape and SX substrate orientation are known. The dendrite tip velocity $V_{hkl}$ is calculated with the relationship:

$$V_{hkl} = S\frac{\cos\theta}{\cos\psi} \quad (1)$$

where S = travel speed, θ = the angle between the travel speed direction S and the interface normal, and ψ = the angle between the interface normal and the active dendrite growth direction.

Current approaches to predict SG formation in weld structures stem from models originally developed to describe the columnar-to-equiaxed transition (CET) in castings (Ref. 2). The model has been applied to the case of fusion welding, and the equation used to calculate the SG area

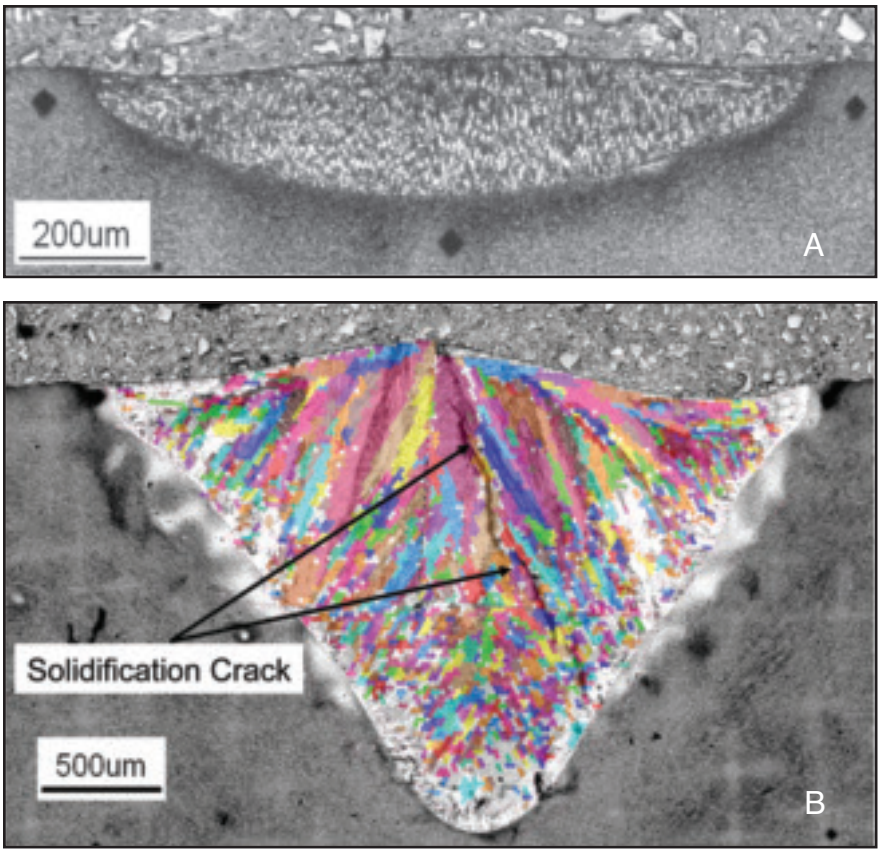


*Fig. 1 — Two EB weld microstructures with superimposed OIM maps. A — 500 W, 95 mm/s; B — 1500 W, 25 mm/s.*

fraction ($\phi$) is given by (Ref. 3)

$$\phi = 1 - \exp\left(-\frac{4\pi N_o}{3}\left(\frac{1}{(n+1)(G^n / aV)^{1/n}}\right)^3\right) \quad (2)$$

where $N_o$ = the nuclei density and both a and n are material constants. The nuclei density is a critical factor because stray grains nucleate independently in the liquid. Estimates of $N_o$ have been made based on SG measurements (Ref. 3). The incidence of SG formation has also been related to the presence of a wide solidification temperature range, $\Delta T_S$ (Ref. 4). Recent solidification studies of Alloy CMSX-4 suggest a solidification temperature range of ~200°C (360°F) based on a Scheil analysis (Ref. 5). However, more detailed modeling has demonstrated that the Scheil model overestimates $\Delta T_S$, and the true value of $\Delta T_S$ for this alloy is about 80°C (Ref. 5).

### Solidification Cracking

Weld solidification cracking in the fusion zone of Ni-based alloys has been the subject of considerable investigation and the mechanism is generally well understood. As is characteristic of weld solidification cracking in other systems, cracks form during the terminal stages of solidification when liquid films are distributed along solidification grain boundaries and, in some cases, interdendritic sites. At this stage, shrinkage strains across the partially solidified boundaries can become appreciable. If the terminal liquid is distributed along the boundaries as a continuous film, the strains cannot be accommodated and the boundaries separate to form a crack. Susceptibility to weld solidification cracking is a function of both metallurgical factors and the level of local strain present at the end of solidification. In terms of metallurgical factors, it is well established that the solidification temperature range as well as the amount and distribution of the interfacial terminal liquid are the primary factors that control solidification cracking susceptibility of Ni-based alloys (Refs. 6–8). Solute redistribution plays an important role in solidification cracking as it affects the solidification temperature range and amount of terminal liquid.

The effect of the solidification temperature range can be understood in simplified terms by considering its influence on the size of the solid + liquid (mushy) zone. During welding, the mushy zone trails behind the liquid weld pool. It is this mushy region that is susceptible to cracking under the influence of shrinkage strain and external restraint. For a fixed temperature gradient in the mushy zone (constant processing parameters), alloys with relatively high solidification temperature ranges can be susceptible to cracking due to a rather large crack-susceptible mushy zone.

The actual distance a solidification crack propagates through the mushy zone depends on the distribution of terminal liquid that exists near the end of the solid + liquid region (Ref. 8) and the level of local strain present. When the amount of terminal liquid is moderate (typically between approximately 1 and 10 vol-% (Ref. 8)) and/or the surface tension is low, the liquid tends to wet the boundary and form a continuous film. This type of morphology is most detrimental as it interferes with the formation of solid/solid boundaries, thus reducing the ability of the material to accommodate strain. When the amount of terminal liquid is relatively high, (greater than approximately 10 vol-%), it can often flow into the cracks and provide a "crack healing" effect (Ref. 8).

Since solidification cracking in superalloys is primarily associated with grain boundaries, SX weld zones have typically been observed to crack when SG formation has introduced grain boundaries into the weld metal. The large $\Delta T_S$ combined with the relatively small grain boundary surface area make these areas especially susceptible to cracking. Moreover, the character of the grain boundary itself can contribute toward cracking susceptibility. High-angle boundaries are more likely to crack than low-angle boundaries due to the prolonged time interval that these boundaries require to coalesce (Ref. 9). While substrate preheating can be used to help reduce the restraint and possibly reduce cracking tendency (Ref. 10), it also reduces the overall G/V ratio in the weld zone, making a columnar-to-equiaxed transition (CET) far more likely to occur. The resultant nucleation and growth of equiaxed grains will significantly increase the solidification cracking susceptibility. Since solidification cracks have never been observed without SG, the avoidance of such cracks can be achieved by reducing or eliminating SG formation. Past studies (Ref. 11) have shown that weld parameters that produce higher G/V ratios can effectively eliminate solidification cracking.

The development and application of heat/fluid flow and solidification modeling techniques for predicting SG formation in welds has recently been described in a companion paper (Ref. 12). In that work, a detailed heat/fluid flow model was first validated for prediction of the melt pool shape and variation in temperature gradient around the melt pool. The heat/fluid flow results were then integrated into a solidification model for determining the ac-

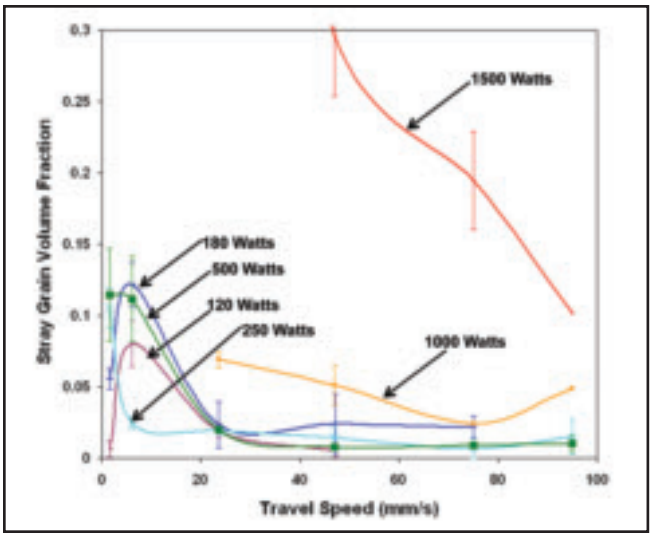


*Fig. 2 — The effect of welding parameters on stray grain area fraction within the electron beam weld structures for the [100]/(100) substrate orientation.*

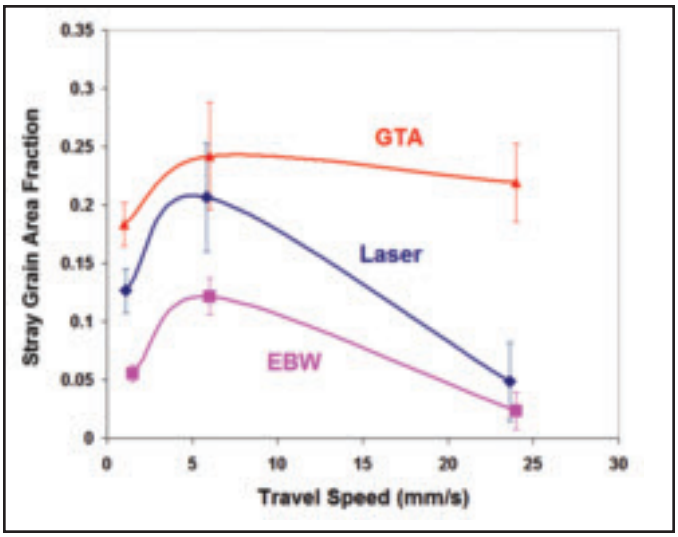


*Fig. 3 — The effect of welding process on stray grain area fraction for an equivalent absorbed power over a range of travel speeds.*

tive growth directions as well as the temperature gradient and solidification velocity along the dendrite growth direction as an aid to predicting conditions that lead to the formation of stray grains. Details of the modeling approach and validation are explained in that paper (Ref. 12). The general effects of welding parameters, substrate orientation, and welding process type on the development of stray grains over a wide range of conditions has also recently been investigated and described (Ref. 13). Selected results from the heat/fluid flow and solidification model (Ref. 12) were used to help develop a detailed understanding of these effects. In this paper, experimental results are presented that correlate the process parameters and process type to the SG formation and cracking tendency. The results of this research can be used as the basis for designing processing strategies for successful single crystal welds repairs.

## Experimental Procedure

A series of autogenous welds was prepared in order to study the SG formation behavior and cracking susceptibility as a function of welding parameters and welding process. The Ni-based superalloy CMSX-4 (Table 1) was selected as a representative alloy used in SX applications for its widespread use in the industry. The alloy composition, as measured through wet-chemical techniques, is given in Table 1. Substrates with dimensions 155 × 80 × 6 mm (6.1 × 3.1 × 0.25 in.) were cast such that the (001) crystal plane was parallel to the sample surface. The substrates were solution heat-treated with a schedule used in industrial practice for Alloy CMSX-4 (heated to 1310°C [2390°F]) for 7 h while under vacuum. Electron beam (EB) welds were performed on the CMSX-4 substrates at beam powers up to 1500 W and travel speeds up to 95 mm/s using a large-chamber Leybold-Heraeus EB welding apparatus. The absorbed power of these welds was taken to be equal to the transmitted power by assuming an absorption coefficient of 1.0, since the transfer efficiency of the EB weld process is known to be very high. For comparison, a smaller set of autogenous welds was also conducted using the gas tungsten arc welding (GTAW) process. The particular powers were selected such that the absorbed powers would overlap some of the EB welds after taking into account the arc transfer efficiency of ~0.7 for the GTAW process (Ref. 14). (All power values cited in this work are absorbed powers.) The torch travel speed also ranged from 1 to 100 mm/s (2.4 to 240 in./min), similar to the EB welds. All welds described in this paper were produced in the [100] direction on the (100) plane.

Cross sections from the welds were prepared using standard metallographic techniques. Orientation imaging microscopy (OIM) analysis was conducted using an electron-backscattered diffraction (EBSD) camera on a Hitachi 4300 field-emission-gun scanning electron microscope (FEG-SEM) in order to determine the area of SG. The weld structures were then revealed by immersing the specimens for 5 s in a reagent consisting of 50 mL of HCl, 50 mL of $H_2O$, and 2.5 g of $CuCl_2$. Light optical microscopy (LOM) photomicrographs of the weld cross sections were used to measure the weld pool dimensions and the fusion zone area. The SG area fraction was determined by dividing the SG area (determined via OIM) by the fusion area (determined by LOM). The average of three different cross sections was acquired for each weld condition. A more thorough description of the experimental weld trials and analysis is provided in separate papers (Refs. 12, 13).

## Results and Discussion

Figure 1 contains typical examples of OIM-generated grain maps superimposed upon the LOM photomicrographs of EB weld microstructures from which they were collected. In these figures, stray grains are identified by the color pixels. The weld structure shown in Fig. 1A resulted from a relatively low heat input (500

**Table 1 — The Composition of the Base Metal CMSX-4 Used in this Study. All values in wt-%.**

| | CMSX-4 |
|---|---|
| Ni | Bal |
| C | 0.002 |
| Cr | 6.36 |
| Co | 9.68 |
| Mo | 0.63 |
| W | 6.34 |
| Ta | 6.52 |
| Ti | 1.00 |
| Al | 5.62 |
| B | 0.0 |
| Zr | 0.0 |
| Hf | 0.10 |
| Re | 2.87 |

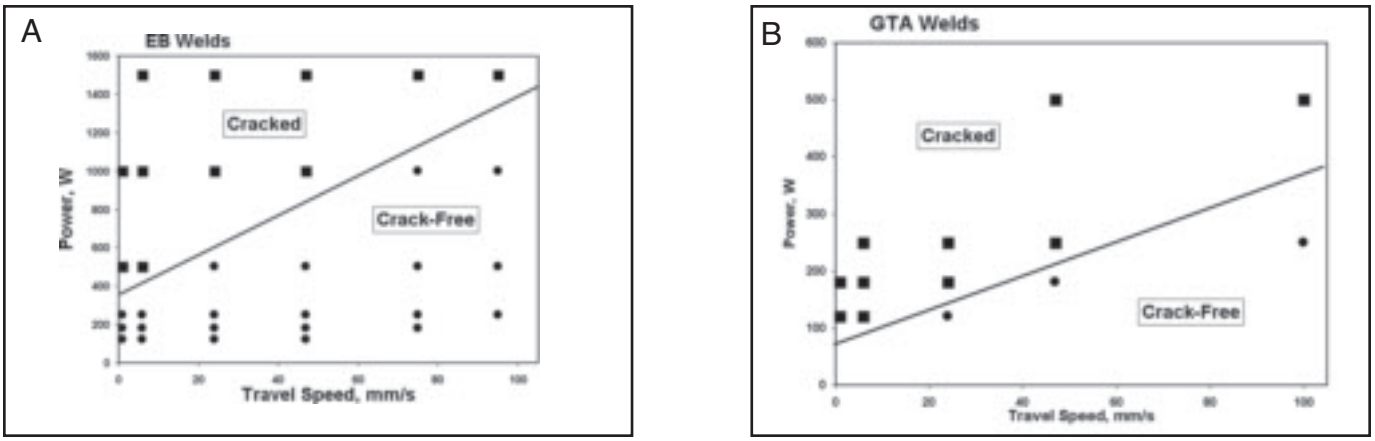


*Fig. 4 — Solidification cracking susceptibility. A — In the EB welds as a function of absorbed beam power and travel speed; B — in the GTA welds as a function of absorbed power and travel speed.*

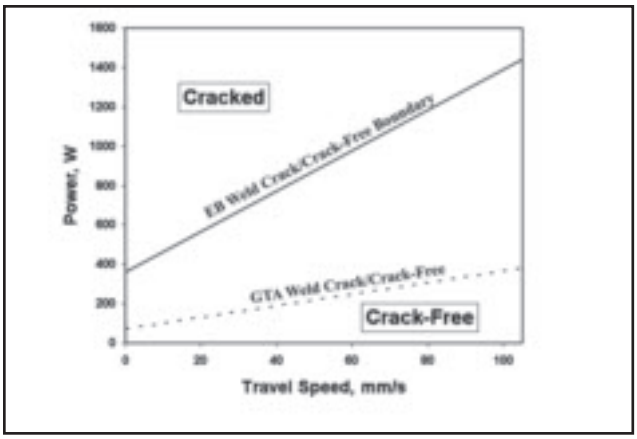


*Fig. 5 — Comparison of crack/crack-free processing regimes for the EB and GTA welds.*

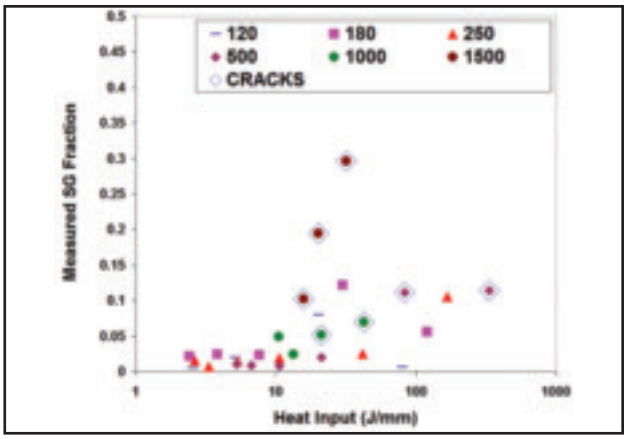


*Fig. 6 — Effect of heat input on the stray grain area fraction and solidification cracking susceptibility in EB welds.*

W, 95 mm/s) and represents a crack-free weld with essentially no SG. By comparison, a high heat input (1500 W, 25 mm/s) EB weld is shown in Fig. 1B. This weld exhibited a high SG content of 70%. The presence of a solidification crack is illustrated by a line of black pixels and is bordered on both sides by stray grains.

While stray grain formation behavior is directly a function of local solidification parameters, these values are functions of the overall welding parameters. Figure 2 shows the overall SG area fraction as a function of beam power and travel speed for the EB welds. (SG measurements were not made at travel speeds below 20 mm/s for welds made at power levels of 1000 and 1500 W because the welds were very large and required long sampling times. In addition, simple metallographic inspection indicated that these large welds had high SG contents.) The maximum SG area fraction is reached at an intermediate travel speed of ~ 6 mm/s. Beyond this value, the SG content decreases with increasing travel speed. This variation in SG content with travel speed has been observed in other work (Ref. 4) and can be explained based on the relative increases in temperature gradient and growth rate with changes in travel speed. When the travel speed is low, initial increases in the speed will cause an increase in the growth rate with only minor changes in the temperature gradient. As a result, the G/V ratio generally decreases, and the amount of SG will therefore increase. Further increases in the travel speed will induce larger increases in the temperature gradient, and, according to Equation 2, G has a larger effect on SG formation than V. Thus, SG formation will subsequently decrease with further increases in the travel speed. The negative influence of increasing weld power on SG formation can be understood by considering its effect on the temperature gradient. An increase in the power will produce a decrease in the temperature gradient, thus promoting more SG to form in the weld.

A limited set of SG measurements was performed on the GTA weld structures. Those results are shown in Fig. 3 along with data from welds conducted using the EB processes at an equivalent absorbed power of 180 W. Data for several laser welds made at an equivalent absorbed power are also shown for comparison (Refs. 12, 13). Note that the GTA welds always exhibit more SG than the EB welds, and the laser welds are intermediate to these two cases. It is interesting to note that the trend in SG content between the three processes correlates to the differences in energy density. The energy density of the heat source influences the temperature gradient in the weld pool, where welds produced with higher energy density processes will experience higher temperature gradients. Thus, welds produced with higher energy density processes are expected to exhibit lower SG contents than welds made from lower energy density processes at equivalent levels of input power and travel speed. This accounts for the relatively high SG grain content of the GTA welds.

Figure 4 summarizes the cracking sus-

ceptibility of all the EB (Fig. 4A) and GTA (Fig. 4B) welds as a function of absorbed power and travel speed. These results clearly show that crack-free welds are promoted by low heat inputs (i.e., low power and high travel speed). This result is not surprising considering the influence of processing parameters on SG formation, and the link between SG formation and cracking susceptibility. Since SG can generally be reduced under low heat input conditions, the cracking susceptibility will also be reduced as the heat input is decreased. The reduced heat input may also be beneficial due to its effect on solidification shrinkage and size of the crack-susceptible mushy zone. The smaller welds produced under lower heat input conditions will exhibit reduced strain from solidification shrinkage along with a smaller crack-susceptible mushy zone, and these factors may also contribute to the reduced cracking susceptibility. It should also be noted that the formation of SG does not directly indicate that cracking will occur. Crack-free welds can be made when SG are present if the mechanical stress and strain for crack formation is low enough. It is also important to note that the low heat input welds are generally wide and shallow, relative to the higher heat input welds that are typically deeper and more narrow. An example of this is readily available by inspection of the two welds shown in Fig. 1. Thus, deeply penetrating welds should generally be avoided when SG and solidification cracking are important to eliminate.

Careful examination of Fig. 4 indicates there is a significant difference in the range of processing parameters between the two processes that can be used to produce crack-free welds. This is shown in Fig. 5, which compares the position of the crack/crack-free boundary for each process. Although the positions of these boundaries are only approximate and apply only to the conditions used in this investigation, the results clearly demonstrate the beneficial effect of the EB process over the GTA process. Reference to Fig. 3 indicates this can likely be attributed to differences in power density and resultant temperature gradient. The higher power density and temperature gradient of the EB process reduces the SG content and, therefore, helps reduce the incidence of cracking.

As previously mentioned, successful weld repair of single crystal turbine blades requires minimizing both the amount of SG and solidification cracks. Fortunately, a reduction of the SG content typically leads to crack-free welds, and each defect, in turn, can be minimized by reductions in the heat input. In view of this, Fig. 6 summarizes the influence of heat input on SG area fraction and cracking susceptibility for the EB welds. These results show that, for the current conditions, there is a critical heat input of ~ 13 J/mm. Welds made below this heat input level are consistently crack-free with very low SG contents (< 5%). Above this value, the formation of SG and associated solidification cracks are more erratic. It is important to note that effective weld repairs can still be accomplished when small amounts of SG form. Welds produced with small amounts of SG typically exhibit a very shallow layer of SG near the top of the weld at the centerline, since G/V is the lowest in that location (Ref. 15). Most practical repairs require the deposition of multiple layers. Thus, the shallow layer of SG can be removed by subsequent passes as long as the depth of melting from the next pass is greater than the depth of stray grains from the preceding pass. With this approach, the SG can be "pushed" up to the final layer, where they can be easily removed by machining. This approach has recently been applied to successfully prepare a 12-layer single crystal deposit using the laser-engineered net shaping process (Ref. 15).

## Conclusions

Autogenous welds were prepared on the single crystal CMSX-4 using the EB and GTA welding processes. The stray grain (SG) area fraction and cracking susceptibility were determined and correlated to the processing parameters and process type. The following conclusions can be drawn from this work:

1) The SG content initially increases and then decreases with increasing travel speed. This effect is attributed to the complex relationship of travel speed on the temperature gradient and growth rate. Stray grain content decreases with decreasing weld power. In general, the SG content and cracking susceptibility can be reduced by welding at low heat inputs.

2) The SG content and corresponding cracking susceptibility was higher for welds prepared with the GTA process compared to the EB process. This difference is attributed to differences in power density and temperature gradient, where the EB process produces a higher temperature gradient that leads to reduced SG and less solidification cracking.

3) For the conditions evaluated in this work, EB welds produced at heat inputs below ~13 J/mm produced welds that were crack-free with very low SG contents (< 5%).

*Acknowledgments*

The authors would like to acknowledge the financial support of the National Science Foundation through Grant No. 0500254. The SX substrates used for welding trials were cast by Howmet, a division of Alcoa, Inc. The EB welding experiments were made possible by Thomas Lienert and Paul Burgardt of Los Alamos National Laboratories.

*References*

1. Park, J.-W., Babu, S. S., Vitek, J. M., Kenik, E. A., and David, S. A. 2003. Stray grain formation in single crystal Ni-base superalloy welds. *Journal of Applied Physics* 94: 4203–4209.

2. Hunt, J. 1984. Steady state columnar and equiaxed growth of dendrites and eutectic. *Materials Science and Engineering* 65: 75–83.

3. Gaumann, M., Bezencon, C., Canalis, P., and Kurz, W. 2001. Single-crystal laser deposition of superalloys: Processing — microstructure maps. *Acta Materialia* 49: 1051–1062.

4. Vitek, J. M., Babu, S. S., David, S. A., and Park, J.-W. 2003. Microstructure development in single crystal welds. *Materials Science Forum* 426–432, 4123–4128.

5. Walter, C., Hallstedt, B., and Warnken, N. 2005. Simulation of the solidification of CMSX-4. *Materials Science and Engineering A* 397, 385–390.

6. Cieslak, M. J. 1991. The welding and solidification metallurgy of Alloy 625. *Welding Journal* 70(2): 49–56.

7. DuPont, J. N., Michael, J. R., and Newbury, B. D. 1999. Welding metallurgy of Alloy HR-160. *Welding Journal* 78(12): 408–414.

8. DuPont, J. N., Robino, C. V., and Marder, A. R. 1998. Solidification and weldability of Nb-bearing superalloys. *Welding Journal* 77(10): 417–431.

9. Wang, N., Mokadem, S., Rappaz, M., and Kurz, W. 2004. Solidification cracking of superalloy single- and bi-crystals. *Acta Materialia* 52: 3173–3182.

10. Kou, S. 2003. *Welding Metallurgy*, John Wiley & Sons, Inc., Hoboken, N.J.

11. Vitek, J. M., Babu, S. S., David, S. A., Park, J.-W., Hu, Y., and Hehmann, W. 2005. Cracking behavior in nickel-based single crystal superalloy welds. *Proceedings of the 7th International Conference on Trends in Welding Research*.

12. Anderson, T. D., DuPont, J. N., and Deb Roy, T. 2010. Origin of stray grain formation in SX superalloy weld pools from heat transfer and fluid flow modeling. *Acta Materialia*, Vol. 58, pp. 1441–1454.

13. Anderson, T. D., DuPont, J. N., and Deb Roy, T. 2010. Stray grain formation in welds of single crystal Ni-base superalloy CMSX-4. *Metallurgical and Materials Transactions A*, 41(1): 181.

14. DuPont, J. N., and Marder, A. R. 1995. Thermal efficiency of arc welding processes. *Welding Journal* 74(12): 406–416.

15. Liu, W., and DuPont, J. N. 2005. Direct laser deposition of a single-crystal Ni3Al-based IC221W alloy. *Metallurgical and Materials Transactions A* 36A(12): 3397–3406A.